Article

Cell Reports

Synaptic Ribbons Require Ribeye for Electron Density, Proper Synaptic Localization, and Recruitment of Calcium Channels

Graphical Abstract

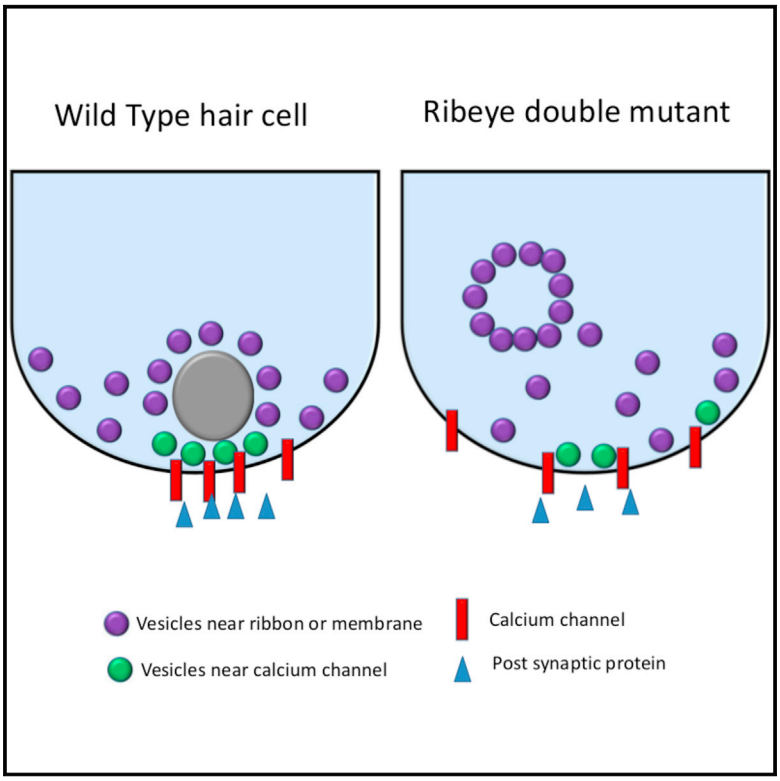

Authors

Caixia Lv, William J. Stewart, Otar Akanyeti, ..., Lavinia Sheets, James C. Liao, David Zenisek

Correspondence

david.zenisek@yale.edu

In Brief

Synaptic ribbons are features of the auditory, vestibular, and visual systems that hold vesicles close to release sites in sensory cells. Lv et al. now find that genetic reduction of Ribeye levels in zebrafish results in the disruption of synaptic ribbon localization and morphology with minor effects on kinetics or levels of vesicle exocytosis.

Highlights

- Ribeye is needed for electron density to form at hair cell synaptic ribbons
- Ribeye mutants have smaller synaptic vesicles and mislocalized ribbons
- Ribeye is required for synaptic ribbon association with calcium channels
- Continuous exocytosis is enhanced in ribeye mutants despite ribbon mislocalization

Lv et al., 2016, Cell Reports *15*, 1–12
June 21, 2016
http://dx.doi.org/10.1016/j.celrep.2016.05.045

CellPress

Please cite this article in press as: Lv et al., Synaptic Ribbons Require Ribeye for Electron Density, Proper Synaptic Localization, and Recruitment of Calcium Channels, Cell Reports (2016), http://dx.doi.org/10.1016/j.celrep.2016.05.045

Cell Reports
Article

Synaptic Ribbons Require Ribeye for Electron Density, Proper Synaptic Localization, and Recruitment of Calcium Channels

Caixia Lv,[1] William J. Stewart,[5] Otar Akanyeti,[5] Courtney Frederick,[1] Jie Zhu,[1] Joseph Santos-Sacchi,[1,3,4] Lavinia Sheets,[6,7] James C. Liao,[5] and David Zenisek[1,2,*]
[1]Department of Cellular and Molecular Physiology
[2]Department of Opthalmology and Visual Sciences
[3]Department of Surgery (Otolaryngology)
[4]Department of Neuroscience
Yale University School of Medicine, New Haven, CT 06520-8066, USA
[5]The Whitney Laboratory for Marine Bioscience and Department of Biology, University of Florida, St. Augustine, FL 32080, USA
[6]Eaton-Peabody Laboratory, Massachusetts Eye and Ear Infirmary, Boston, MA 02114, USA
[7]Department of Otolaryngology, Harvard Medical School, Boston, MA 02114, USA
*Correspondence: david.zenisek@yale.edu
http://dx.doi.org/10.1016/j.celrep.2016.05.045

SUMMARY

Synaptic ribbons are structures made largely of the protein Ribeye that hold synaptic vesicles near release sites in non-spiking cells in some sensory systems. Here, we introduce frameshift mutations in the two zebrafish genes encoding for Ribeye and thus remove Ribeye protein from neuromast hair cells. Despite Ribeye depletion, vesicles collect around ribbon-like structures that lack electron density, which we term "ghost ribbons." Ghost ribbons are smaller in size but possess a similar number of smaller vesicles and are poorly localized to synapses and calcium channels. These hair cells exhibit enhanced exocytosis, as measured by capacitance, and recordings from afferent neurons post-synaptic to hair cells show no significant difference in spike rates. Our results suggest that Ribeye makes up most of the synaptic ribbon density in neuromast hair cells and is necessary for proper localization of calcium channels and synaptic ribbons.

INTRODUCTION

Primary sensory cells of the auditory, vestibular, and visual systems encode sensory information as graded changes in voltage that lead to graded changes in glutamate release. These non-spiking cells use synaptic ribbons, which hold a dense array of synaptic vesicles in active zones near release sites. Because these cells exhibit tonic and graded signaling in response to sensory stimuli, it has largely been assumed that the synaptic ribbon is necessary to carry out this task (Matthews and Fuchs, 2010). Indeed, ribbon-synapse-containing cells have been demonstrated to exhibit a sustained phase of exocytosis in response to prolonged stimuli (Lagnado et al., 1996; Parsons et al., 1994; Moser and Beutner, 2000; Edmonds et al., 2004; Bartoletti et al., 2010), and optical studies have revealed that vesicles are immobilized to and move along the ribbon in response to stimuli (Vaithianathan et al., 2016; Zenisek, 2008; Zenisek et al., 2000; Midorikawa et al., 2007).

The most abundant protein in the synaptic ribbon is Ribeye, a protein arising from an alternative start site at the gene encoding for the CtBP2 transcriptional co-repressor (Schmitz et al., 2000). Ribeye can be subdivided into two domains, a ribbon-specific A-domain and a B-domain, which is nearly identical to CtBP2 (Schmitz et al., 2000).

Genetic deletion of mouse Ribeye leads to a loss of synaptic ribbons in the retina, which is accompanied by a reduction in synaptic transmission from bipolar cells without observable changes in the kinetic features of release (Maxeiner et al., 2016), whereas morpholino-oligonucleotide (MO)-driven knockdown of Ribeye expression leads to the mislocalization of calcium channels (Sheets et al., 2011; Lv et al., 2012) and a reduction of spiking rates in afferent neurons postsynaptic to zebrafish hair cells (Sheets et al., 2011).

To better understand the function of Ribeye and the synaptic ribbon, we used genome editing to introduce frameshifting mutations in the A-domain of both zebrafish Ribeye-encoding genes and used light and electron microscopy (EM), whole-cell capacitance measurements, and recordings from afferent neurons to measure the effects on neuromast hair cells. The resultant double-homozygous mutant animals exhibited dramatically reduced Ribeye levels in hair cells, leading to a loss of electron density from hair cell ribbons, shrinkage of ribbon size, mislocalization of ribbon-like structures, and disruption in the association of calcium channels with the ribbon. Despite these changes, the continuous phase of exocytosis is enhanced, and we could not detect differences in afferent neuron response in mutant animals. These results indicate that Ribeye likely makes up the electron-dense portion of the ribbon and recruits calcium channels to release sites in zebrafish hair cells but is not required for vesicle binding, transport, or maintaining continuous release.

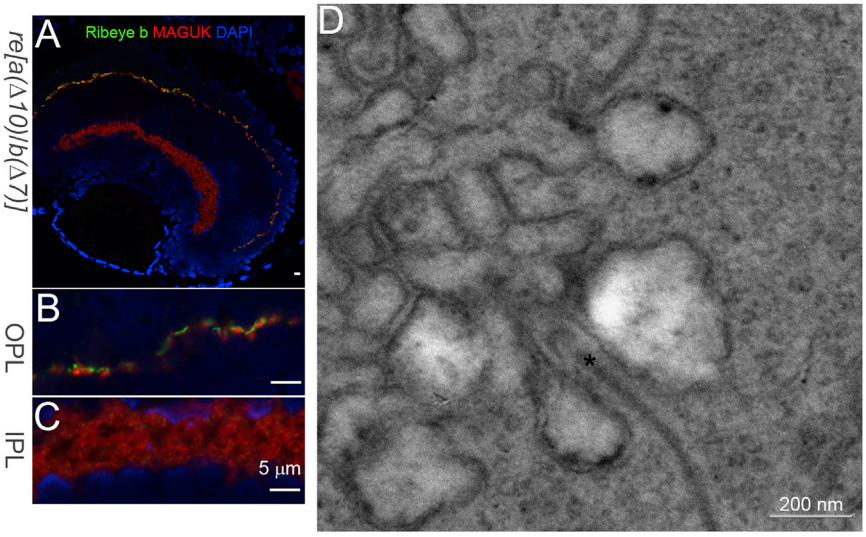

Figure 1. Ribeye and Synaptic Ribbons Remain in the Retina of *ribeye a(Δ10)/ ribeye b(Δ7) (re[a(Δ10)/b(Δ7)])* double homozygous mutants.

(A) Confocal image of Ribeye b (green) and post-synaptic maker MAGUK (red) staining in 5-dpf *re[a(Δ10)/b(Δ7)]* homozygous mutants. DAPI (blue) stains for the nucleus. Scale bar, 5 μm.

(B) 3× magnification of outer plexiform layer staining in 5-dpf *re[a(Δ10)/b(Δ7)]* homozygous mutants retina. Scale bar, 5 μm.

(C) 3× magnification of inner plexiform layer staining in 5-dpf *re[a(Δ10)/b(Δ7)]* homozygous mutants retina. Scale bar, 5 μm.

(D) Electron micrograph of photoreceptor ribbon from 5-dpf *re[a(Δ10)/b(Δ7)]* homozygous mutant retina. Scale bar, 200 nm.

RESULTS

Generation of Targeted Zebrafish *ribeye* Mutants

To study Ribeye function, we first generated a line of zebrafish harboring mutations in the ribbon-synapse-specific A-domain of Ribeye a that leads to frameshifts resulting in a premature stop codon using zinc finger nucleases (ZFNs) (Supplemental Experimental Procedures; Figure S1). One such mutant that led to a 10-bp deletion (*ribeye a*(Δ10)) was bred to homozygosity for further experiments. Figure S2 shows immunostaining of retinal sections of wild-type (WT) and *ribeye a*(Δ10) homozygous fish with antibodies against Ribeye a or Ribeye b or with a CtBP antibody that labels CtBP1, CtBP2, and all isoforms of Ribeye. As expected, CtBP and Ribeye b staining was still evident in the *ribeye a(Δ10)* homozygous animals, due to expression of Ribeye b. Note that, while the CtBP expression level is greatly reduced in the inner plexiform layer (IPL), the CtBP staining in the outer plexiform layer (OPL) is similar in the *ribeye a*(Δ10) homozygous and WT animals, consistent with stronger expression of Ribeye b in photoreceptor terminals and higher expression of Ribeye a in bipolar cells. EM images revealed normal-appearing ribbons in both the retina and lateral line of *ribeye a*(Δ10) homozygous animals (data not shown). We found that animals homozygous for these mutations are viable and do not exert obvious sensory phenotypes.

Next, we targeted *ribeye b* using CRISPR/Cas9 (clustered regularly interspaced short palindromic repeats/CRISPR-associated protein 9)-based constructs. Using this strategy, we generated eight lines of fish harboring mutations in this region of *ribeye b*, which led to premature stop codons (Figure S1C). As with the ZFN-generated mutations of *ribeye a*, the mutations introduced into *ribeye b* are expected to cause a truncation of the sequence in the A-domain, with no effect on CtBP2 expression.

Characterization of *ribeye a(Δ10)/ribeye b(Δ7)* Homozygous Zebrafish

Next, we characterized the *ribeye a(Δ10)/ribeye b(Δ7)* (hereinafter termed *re[a(Δ10)/b(Δ7)]*) double-homozygous mutants at the level of light and EM in the retina and in hair cells of the lateral line. Surprisingly, double-homozygous mutants were immunopositive for CtBP and Ribeye b in the OPL of the retina, indicating that at least some Ribeye continues to be expressed, despite the mutations (Figure 1). Consistent with Ribeye expression, EM revealed that synaptic ribbons were also present in the OPL of *re[a(Δ10)/b(Δ7)]* fish (Figure 1D).

In contrast to the retina findings, Ribeye was found to be dramatically reduced in the hair cells of zebrafish neuromasts at 5 days postfertilization (dpf) (Figure 2). Figures 2A and 2B show results from neuromasts that are labeled for Ribeye a (Figure 2A) or Ribeye b (Figure 2B) with pan-MAGUK, a marker for post-synaptic densities that labels afferent post-synaptic structures in afferent fiber terminals (Sheets et al., 2011; Meyer et al., 2005). In WT animals, pan-MAGUK staining was found to colocalize near bright spots immunopositive for Ribeye a (Figure 2A, left) and Ribeye b (Figure 2B, left). By contrast, *re[a(Δ10)/b(Δ7)]* double homozygotes exhibit little staining for Ribeye a (Figure 2A, right) but continued to exhibit staining for pan-MAGUK (Figures 2A and 2B, right). Some residual fluorescent spots remained in double-homozygous mutant animals. The Ribeye a puncta were reduced in number from 2.5 ± 0.18 in WT fish to 1.5 ± 0.3 in double homozygotes (Figure 2D), and in intensity from 15,728 ± 1,517 to 6,369 ± 1,021 (Figure 2E). Ribeye b was not detectable (Figure 2B). Though the number of pan-MAGUK spots in double homozygotes was unchanged (Figure 2D), the puncta intensity was significantly reduced (Figure 2E).

Next, we tested whether overall CtBP levels were also reduced from synaptic sites by staining with an antibody that recognizes Ribeye a, Ribeye b, CtBP1, and CtBP2. As with the Ribeye a staining, we found fewer and dimmer CtBP puncta than in control animals. On average, puncta in double homozygotes had an integrated intensity of 17% of WT fish.

Lastly, to determine whether the Ribeye a immunofluorescent (IF) spots properly localized near post-synaptic structures, we measured the distance of the centroid of each Ribeye a spot to its nearest pan-MAGUK spot. Figure 2F plots the results as a cumulative histogram. As can be seen in the figure, spots in mutant animals were found further away from

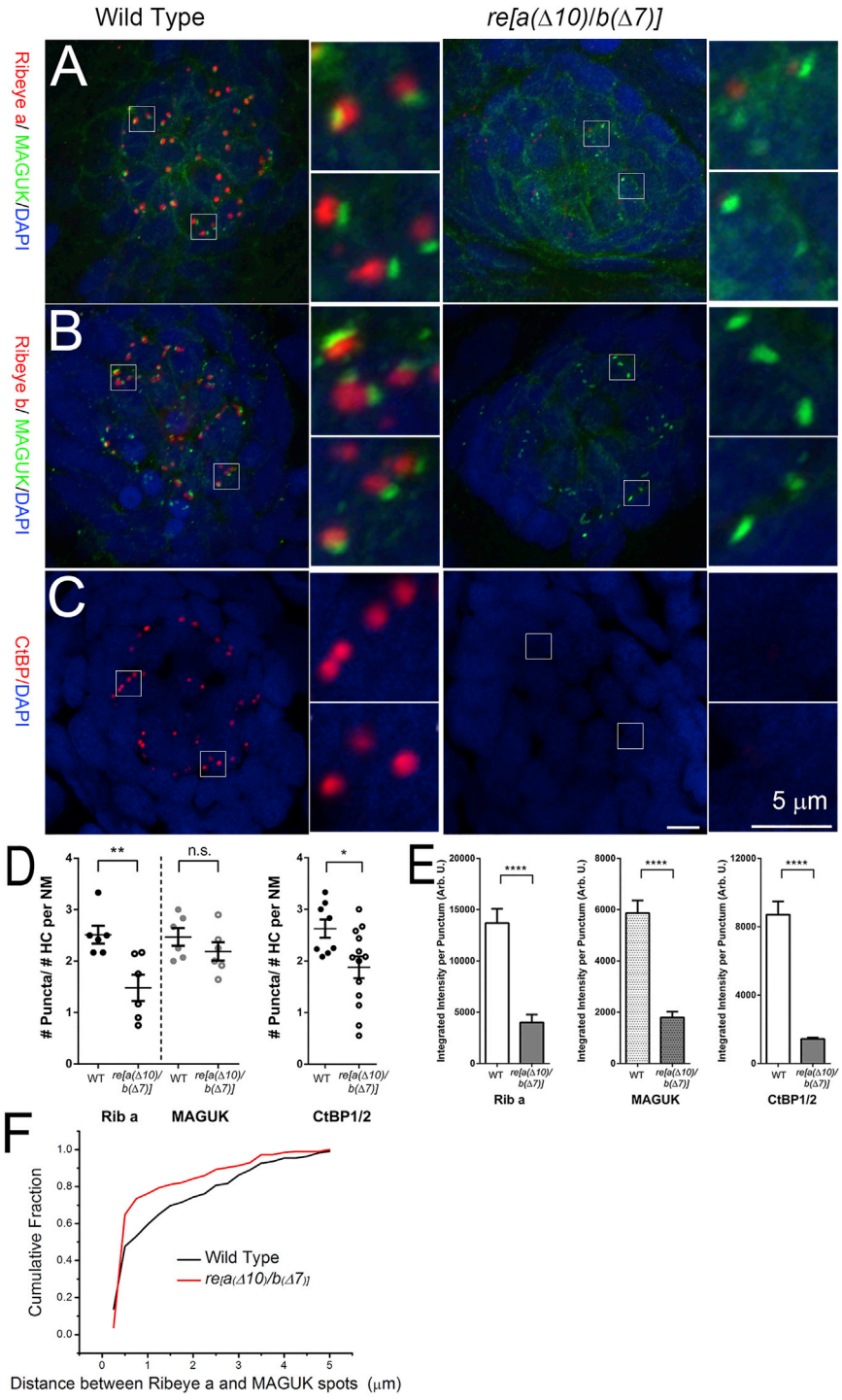

Figure 2. Ribeye Is Dramatically Reduced from Neuromast Hair Cells of *re[a(Δ10)/b(Δ7)]* Double Homozygous Mutants 5 dpf

(A) Confocal images of Ribeye A (red) and post-synaptic density marker pan-MAGUK (green) staining 5 dpf in WT (left) and *re[a(Δ10)/b(Δ7)]* homozygous mutant (right) neuromast. Insets show magnified images centered around synapses. Note the close apposition of Ribeye a and pan-MAGUK in WT animals, whereas little Ribeye a staining is found near pan-MAGUK in the *re[a(Δ10)/b(Δ7)]* double-homozygous mutants.

(B) Ribeye b (red) and pan-MAGUK (green) antibody staining in 5-dpf WT (left) and *re[a(Δ10)/b(Δ7)]* homozygous mutant (right) neuromast.

(C) CtBP antibody staining (green) in 5-dpf WT (left) and *re[a(Δ10)/b(Δ7)]* homozygous mutant (right) neuromast. DAPI (blue) stains nucleus. Scale bars, 5 mm.

(D) The number of Ribeye a, MAGUK, or CtBP1 immunolabeled puncta per hair cell in 5- to 6-dpf WT and *re[a(Δ10/b(Δ7)* mutants. Each circle represents an individual neuromast (NM) within a larva. The number of puncta per hair cell was approximated by dividing the number of Ribeye puncta within an NM by the number of hair cells in the NM. Error bars indicate SEM. Unpaired t test; **p = 0.0075; *p = 0.0226; n.s., not significant.

(E) Integrated intensities per punctum of Ribeye a, MAGUK, and CtBP1. Bars represent the means; error bars indicate SEM. Mann-Whitney U test; ***p < 0.0001, for both mutant alleles.

(F) Cumulative histogram of distances between Ribeye a spots to their nearest pan-MAGUK spot in confocal micrographs for WT (red) and *re[a(Δ10/b(Δ7)]* double-homozygous mutants (black).

post-synaptic densities, suggesting defects in their ability to localize to synapses.

Morphology of Hair Cell Synaptic Ribbons in *re[a(Δ10)/b(Δ7)]* Homozygous Mutants

Neuromast hair cells of WT embryos at 5 dpf exhibit spherical synaptic ribbons that localize near the plasma membrane near afferent fibers (Obholzer et al., 2008). Similarly, we found that EM sections of neuromasts in WT fish exhibited electron-dense synaptic ribbons (n > 20 fish). Figures 3A and 3B show typical electron micrographs of a synaptic ribbon from a WT hair cell, which were localized near afferent neurons separated by two cell membranes. Afferent neurons were identified in electron micrographs by their reduced density, lack of synaptic vesicles, and mitochondria. In WT fish, we found that 41 of 41 ribbons were localized within 70 nm of a visible plasma membrane opposite an afferent neuron. By contrast, we found no ribbons with typical electron-dense centers in *re[a(Δ10)/b(Δ7)]* double homozygotes. Instead, 5-dpf embryos of *re[a(Δ10)/b(Δ7)]* double homozygotes exhibited ribbon-like structures that lacked electron densities but maintained an organized collection of synaptic vesicles in a spherical array (Figures 3C–3F), which we have named "ghost ribbons." While some ghost ribbons appeared to localize adjacent to afferent neurons (Figure 3C; n = 14 of 41 ghost ribbons), most were not found near

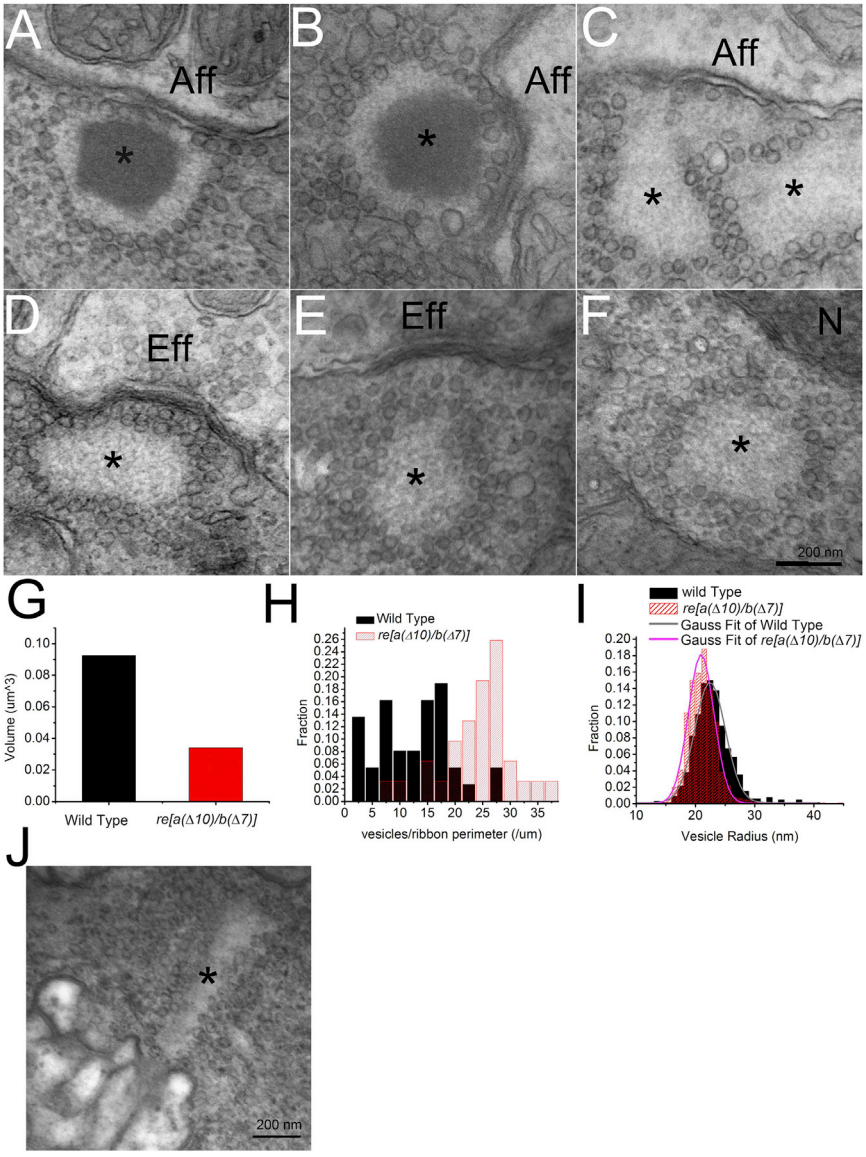

Figure 3. Mutant Zebrafish Exhibit Ribbons Lacking Synaptic Densities in Neuromast Hair Cells

(A and B) Electron micrograph showing typical examples of synaptic ribbons in neuromast hair cells in 5- dpf WT zebrafish (marked by an asterisk). Note prominent density and typical localization near the afferent neuron (Aff).

(C–F) Examples of electron micrographs of ghost ribbons (marked by an asterisk) taken from neuromast hair cells of *re[a(Δ10)/b(Δ7)]* homozygous zebrafish. Note the absence of a synaptic ribbon density with presence of vesicle array. Sone ghost ribbons locate near the afferent neurons (denoted Aff) (C), near the efferent neurons (Eff) (D), far away from the membrane (E), or in the middle of the cell (F). N denotes nucleus. Scale bar, 200 nm.

(G) Volume of ribbon and ghost ribbons in 5-dpf WT and *re[a(Δ10)/b(Δ7)]* homozygous mutant hair cells.

(H) Histogram of vesicle density per length of perimeter of ribbon or ghost ribbon in cross-section in WT and *re[a(Δ10)/b(Δ7)]* homozygous mutants.

(I) Histogram of vesicle size associated with ribbon or ghost ribbon in WT and *re[a(Δ10)/b(Δ7)]* homozygous mutants.

(J) Electron micrograph of ghost-ribbon like structure in the outer plexiform layer of *re[a(Δ10)/b(Δ7)]* double homozygous retina.

identifiable afferent fibers. Figure 3 shows examples of ghost ribbons near efferent neurons (Figure 3D), away from the cell membrane (Figure 3E), and in the center of cell (Figure 3F). By contrast, ribbons of the retina of *re[a(Δ10)/b(Δ7)]* double homozygotes were found to be largely normal; however, we found two examples of structures within photoreceptors of *re[a(Δ10)/b(Δ7)]* double homozygotes that resembled the hair cell ghost ribbons but took on the elongated shape of a photoreceptor ribbon (Figure 3J). These results indicate that Ribeye is necessary for the maintaining the electron density of the ribbon and plays a critical role in localizing ribbons to proper synaptic locations.

Next, we quantified and compared the morphological properties of ghost ribbons in *re[a(Δ10)/b(Δ7)]* double homozygotes to ribbons in WT animals. In WT hair cells (n = 45 ribbons, 18 fish), the area of the region beneath the vesicles, including both the electron density and the surrounding light space (e.g., Figures 3A and 3B), was, on average, 0.163 μm^2. If we assume that the ribbons are roughly spherical and that each image represents a random cross-section of that sphere, WT ribbons would have a cross-section of 0.244 μm^2 at their equator, which yields a spherical ribbon with a diameter of 560 nm and a volume of 0.091 μm^3. The density occupied about 43% of WT ribbons. By contrast, ghost ribbons lacking the density were much smaller (n = 32 ribbons; ten fish), with an estimated cross-sectional area of 0.119 μm^2, equivalent to a 390-nm diameter sphere and a volume of 0.031 μm^3. Hence, when one does not factor in the vesicle volume, the volume of ghost ribbons is only 34% of the volume of WT ribbons, less than the 57% that one would predict if ribbons only lost the density but similar to a previous estimate of the contribution of Ribeye to ribbon volume in retinal bipolar cells using a ribbon-binding peptide (Zenisek et al., 2004).

To analyze the vesicles associated with ribbons and ghost ribbons, we counted the number of vesicles within one vesicle diameter of the ribbon. Despite the smaller area of the ghost ribbons, we observed more vesicles per section associated with ghost ribbons in mutant animals (21.8 ± 1.3) than with ribbons in WT cells (15.7 ± 2.0). To measure the density of vesicles on ribbons, we divided the number of vesicles by the length of the perimeter of the ribbon in each section. On average, we found

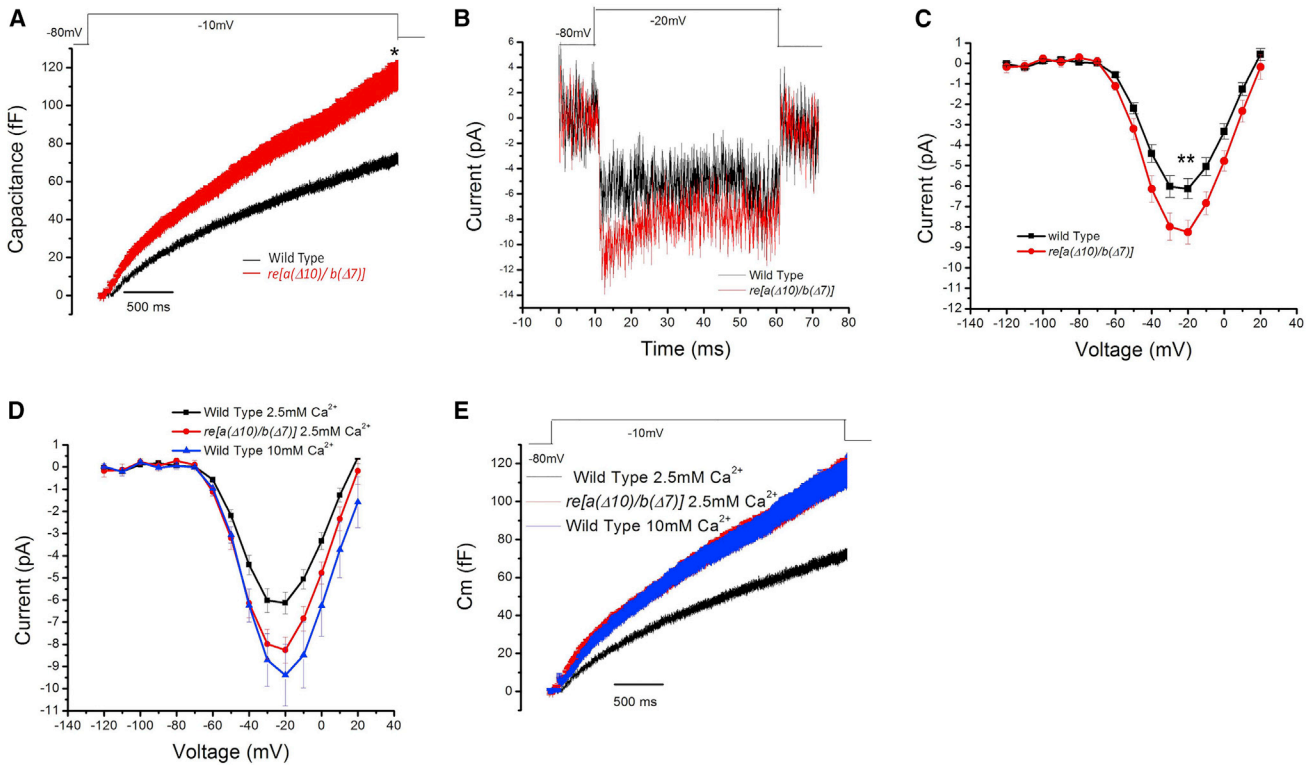

Figure 4. Results from Whole-Cell Voltage-Clamp Recordings from WT and *re[a(Δ10)/b(Δ7)]* Homozygous Mutant Neuromast Hair Cells

(A) Average whole-cell capacitance measurements of WT (black, n = 11) and *re[a(Δ10)/b(Δ7)]* homozygous mutants (red, n = 12) neuromast hair cells in response to 3-s step-depolarizations. Note that all traces include error bars denoting SEM for each condition. The average capacitance increase at the end of the 3-s depolarization (averaged over 100 ms) was 67.8 ± 5.0 fF for the WT hair cells and was 106.1 ± 13.6 fF in the mutants. p = 0.018.

(B) Averaged calcium current trace of WT (black) and *re[a(Δ10)/b(Δ7)]* homozygous (red) mutants in response to a −20-mV step depolarization.

(C) Plot of current-voltage relationship for WT fish NM hair cells (black, n = 15) and *re[a(Δ10)/b(Δ7)]* homozygous mutant neuromast hair cells (red, n = 17). At −20 mV, the average current in WT cells was −6.1 ± 0.5 pA, and mutant fish cells was −8.3 ± 0.6 pA. p = 0.010. The fish recorded were between 5 and 8 days old, and the neuromasts recorded were P3 and P4.

(D) Capacitance recording of WT fish at 2.8 mM Ca^{2+} (black) and 10 mM Ca^{2+} (blue) external solution and double-mutant fish at 2.8 mM Ca^{2+} external solution (red) in response to a 3-s step depolarization. The average capacitance increase at the end of the 3-s depolarization (averaged over 100 ms) was 105.09 ± 13.74 fF for the WT hair cells at 10 mM Ca^{2+} solution. Capacitance increases in WT and double-mutant fish in 2.8 Ca^{2+} external solution are the same as in (A).

(E) Plot of current-voltage relationship of WT fish at 2.8 mM Ca^{2+} (black) and 10 mM Ca^{2+} (blue) external solution, and double-mutant fish at 2.8 mM Ca^{2+} external solution (red). At −20 mV, the calcium current of WT fish in 10 mM Ca^{2+} external solution is −9.39 ± 1.40 pA, compared to double-mutant fish in 2.8 mM Ca^{2+} external solution is 8.26 ± 0.58 pA.

22.7 ± 1.0 vesicles per micrometer perimeter in mutant ghost ribbons and 11.1 ± 0.9 vesicles per millimeter in images of ribbons of WT animals. Even after the removal of a subset of WT ribbons that had very few vesicles (five or less), the vesicle density on ribbons remained lower in the WT cells (13.0 ± 0.8 μm^{-1}). Figure 3H plots a histogram of these values for both genotypes. To estimate the effect on overall vesicle number, we estimated the area of ribbon assayed in each 80-nm section relative to the total ribbon surface area using our spherical assumption. Based on this method, we calculated an estimate of 133 ± 17 vesicles per ribbon in WT animals and 129 ± 8 associated with ghost ribbons in *re[a(Δ10)/b(Δ7)]* double-mutant animals.

Lastly, we measured the size of the vesicles associated with ribbons and ghosts. We measured the size of vesicles associated with ribbons (n = 671) and ghost ribbons (n = 627). On average, ribbon-associated vesicles in WT animals had an average area of 1,631 ± 15 nm^2, whereas vesicles in *re[a(Δ10)/b(Δ7)]* were 1,437 ± 12 nm^2. Since the vesicles are round in the images, we converted the areas into vesicle radii and plotted the results as a histogram in Figure 3I. While the difference in vesicle size is small (21.4 ± 0.09 in double homozygotes versus 22.4 ± 0.1 nm in WT), the differences are highly significant ($p < 0.003$ when comparing averages across ribbons).

re[a(Δ10)/b(Δ7)] Double Mutants Exhibit Enhanced Exocytosis and Calcium Current

Next, we tested the release properties of the *re[a(Δ10)/b(Δ7)]* double-homozygous animals and WT animals. To do so, we performed whole-cell membrane capacitance recordings in response to long step depolarizations in both WT and *re[a(Δ10)/b(Δ7)]* double-homozygous fish 5–8 dpf, using a two-sine approach that allows for measuring exocytosis during a depolarization (Ricci et al., 2013; Schnee et al., 2011). Figure 4A, shows the average responses of 11 WT hair cells and 12 *re*

Please cite this article in press as: Lv et al., Synaptic Ribbons Require Ribeye for Electron Density, Proper Synaptic Localization, and Recruitment of Calcium Channels, Cell Reports (2016), http://dx.doi.org/10.1016/j.celrep.2016.05.045

Table 1. Best-Fit Values of Hair Cell Capacitance Measurements from WT and Mutant Zebrafish

	Linear Phase, β (fF/s)	Amplitude, A (fF)	Time Constant, τ (ms)
Wild type/1 EGTA/2.8 Ca^{2+}	17.6	18.9	501
Wild type/10 EGTA/2.8 Ca^{2+}	16.7	15.6	622
re[a(Δ10)/b(Δ7)]/1 EGTA/2.8 Ca^{2+}	29.1	19.2	346
re[a(Δ10)/b(Δ7)]/10 EGTA/2.8 Ca^{2+}	8.4	10.5	579
Wild type/1 EGTA/10 Ca^{2+}	28.8	22.7	481

[a(Δ10)/b(Δ7)] fish in response to 3-s voltage steps to −10 mV. WT hair cells exhibited a steady rise in whole-cell capacitance, which could be well fit by the sum of an exponentially asymptoting fast phase and a linear continuous phase, similar to what has been observed in mouse (Moser and Beutner, 2000) and chick (Eisen et al., 2004) cochlear hair cells. To fit the data, the latter half of the capacitance response was fit to a straight line, and a line with that slope was subtracted from the raw data. The residual was then fit by an exponential. Using this approach, the WT response was best fit by a linear phase of 17.6 fF/s and an exponential with an amplitude of 18.9 fF and with a time constant of 501 ms (see Table 1).

Surprisingly, the capacitance response from *re[a(Δ10)/b(Δ7)]* double-homozygous animals showed a larger increase in capacitance in response to step depolarization (Figure 4A; Table 1). The linear phase (65% greater than WT) was specifically enhanced in mutant animals, whereas the exponential amplitude was only minimally larger (1.6% greater than WT). The enhanced exocytosis in double-homozygous mutant zebrafish was accompanied by an increase in the calcium current in the hair cells measured at −20 mV (Figure 4B). Figure 4C shows the average current as a function of membrane potential from WT (n = 15) and *re[a(Δ10)/b(Δ7)]* double-homozygous (n = 17) fish. While the shape of the current-voltage (I-V) relationship appeared similar, the calcium currents were found to be larger in the cells lacking Ribeye. Increasing extracellular calcium to 10 mM in WT animals resulted in an increase in calcium current (Figure 4D) and exocytosis (Figure 4E) to levels that mimicked that of *re[a(Δ10)/b(Δ7)]* double-homozygous animals, suggesting that the enhanced exocytosis can largely be explained by the enhanced calcium current.

Calcium Channels Are Poorly Coupled to Release in *re[a(Δ10)/b(Δ7)]* Double-Homozygous Hair Cells

Next, we performed co-immunofluorescence staining with an antibody for the calcium channel CaV1.3 (Sheets et al., 2011, 2012) and a post-synaptic marker pan-MAGUK (Meyer et al., 2005). In WT animals, CaV1.3 staining revealed spots (Figure 5A, red), which were found localized near pan-MAGUK spots (Figure 5A, green). By contrast, CaV1.3 and pan-MAGUK spots were spatially segregated in *re[a(Δ10)/b(Δ7)]* double homozygotes (Figure 5B), suggesting improper localization.

As a second test for the proximity between calcium channels and active zones, we determined the effect of the slow calcium buffer EGTA on exocytosis in WT and *re[a(Δ10)/b(Δ7)]*double-homozygous mutant animals. High concentrations of EGTA have little effect on calcium concentrations in small nano-domains near the mouth of open calcium channels but efficiently reduce bulk calcium concentrations and calcium at other distal locations away from the channels. Hence, if sites of exocytosis are very near calcium channels, EGTA is expected to have little effect on release. Electrophysiological studies from various synapses have used this method to demonstrate tight proximity of calcium channels to release sites (Mennerick and Matthews, 1996; Adler et al., 1991; Roberts, 1994; Moser and Beutner, 2000; Mehta et al., 2014; Coggins and Zenisek, 2009; Wong et al., 2014). Similarly, WT hair cells showed little change in the amount of exocytosis when 10 mM EGTA was introduced into the cell via patch pipette and stepped to −10 mV, suggesting tight coupling between calcium channels and release sites in these cells (Figure 5C). On average, the capacitance response to a 3-s step depolarization from −80 mV to −10 mV was 67.8 ± 5.0 fF for cells loaded with 1 mM EGTA (n = 11) and 62.8 ± 4.9 fF for cells loaded with 10 mM EGTA (n = 7) with similar kinetics. By contrast, 10 mM EGTA had a dramatic effect on ΔCm in *re[a(Δ10)/b(Δ7)]* double-homozygous hair cells, reducing release by 66% relative to 1 mM EGTA and only 55% of WT hair cells loaded with 10 mM EGTA (Figure 5D; Table 1). The effect of EGTA was more pronounced in the continuous phase (72% reduced) than the exponential phase (33%). These results suggest that Ribeye is required for proper formation of calcium channel/vesicle nanodomains and that the enhanced release observed in *re[a(Δ10)/b(Δ7)]* double homozygotes may arise primarily from vesicles residing outside of calcium channel nanodomains.

Recordings from Afferent Neurons

The aforementioned results indicate that hair cells from *re[a(Δ10)/b(Δ7)]* double homozygotes continue to exhibit robust exocytosis in response to depolarization, despite lacking ribbon densities, but the release is inefficiently coupled to calcium channels, and ribbons are mislocalized. Next, we tested whether ghost-ribbon-containing hair cells could efficiently drive post-synaptic spiking in afferent neurons. To do so, we recorded action potentials from primary afferent neurons of the posterior lateral line system using loose-patch extracellular recordings in response to piezo-electrically driven stimuli directed to the kinocilia of neuromast hair cells (Levi et al., 2015). For these experiments, cells were selected for analysis only if a stimulus was found to generate action potentials in the recorded afferent. Hence, these recordings represent cells that receive synaptic input from hair cells. We could find no differences between WT and mutant animals in their afferent responses. Figure 6 summarizes our results from these recordings in WT and *re[a(Δ10)/b(Δ7)]* double-homozygous animals. Figure 6A shows representative recordings taken from neuromast L1 from a WT animal and a mutant animal stimulated at 60 Hz. As can be observed from the recordings, both the WT and mutant animals showed robust spiking throughout a 10-s stimulus train. We found no difference in the spontaneous spike rate before stimulation for WT and *re[a(Δ10)/b(Δ7)]* double-homozygous fish (Figure 6B). Figure 6C

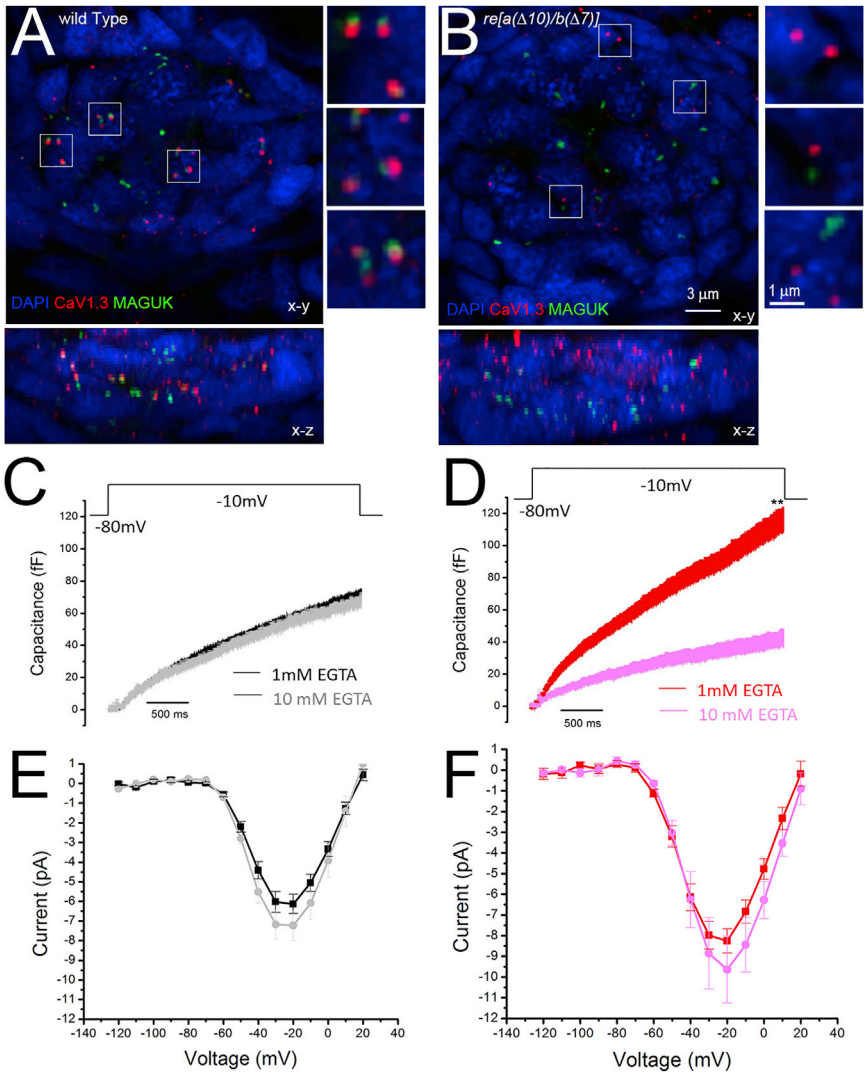

Figure 5. *re[a(Δ10)/b(Δ7)]* Homozygous Hair Cells Have Poorly Localized Calcium Channels and Exhibit Enhanced Sensitivity to 10 mM EGTA

(A and B) Immunolabel of CaV1.3a and MAGUK in 5-dpf WT (A) and *re[a(Δ10)/b(Δ7)]* (B). While Cav1.3 immunolabeled puncta generally localize to the presynapse adjacent to postsynaptic MAGUK immunolabel in WT (A; insets), CaV1.3a clusters fail to localize to the presynapse in *re[a(Δ10/b(Δ7)]* mutants (B; inset).

(C and D) Capacitance increase of WT and double-mutant neuromast hair cells in response to a 3-s step depolarization with 1 mM EGTA or 10 mM EGTA (gray, n = 8) in the internal solution. The average capacitance increase at the end of the 3-s depolarization (averaged over 100 ms) of WT fish was 67.8 ± 5.0 fF at 1 mM EGTA (C; black, n = 11) and 62.8 ± 4.9 fF at 10 mM EGTA (C; gray, n = 7); p = 0.50. 10 mM EGTA blocks 7.4% of release, compared to 1 mM EGTA in WT fish. The average capacitance increase at the end of the 3-s depolarization (averaged over 100 ms) of double mutants was 106.1 ± 13.6 fF at 1 mM EGTA (D; red, n = 12), and 36.3 ± 8.7 fF at10 mM EGTA (D; pink, n = 8), p = 0.01. 10 mM EGTA blocks 66.% of release compared to 1 mM EGTA.

(E and F), Plot of current-voltage relationship for WT fish NM hair cells (E) and *re [a(Δ10)/b(Δ7)]* homozygous mutant neuromast hair cells (F) at 1 mM EGTA and 10 mM EGTA internal solution. At −20 mV, the average current of WT cells was −6.1 ± 0.5 pA at 1 mM EGTA (E; red, n = 15) and 6.9 ± 0.9 (E; pink, n = 8). p = 0.46. The average current of mutant fish cells was −8.26 ± 0.58 pA at 1 mM EGTA solution (F; red, n = 17), and −9.9 ± 2.2 pA at 10 mM EGTA solution (F; pink, n = 6). p = 0.49. The fish recorded were between 5 and 8 days old, and the neuromasts recorded were P3 and P4.

plots the recorded spike frequency that has been time averaged over the 10-s stimulus train for three frequencies (2 Hz, 30 Hz, and 60 Hz). Figure 6F shows the spike rate over the entire 10 s of 60-Hz stimulation for all fish. As can be seen from the plots, *re[a(Δ10)/b(Δ7)]* double-homozygous fish exhibited spike rates similar to WT animals at all frequencies tested. We found no effect of genotype on the ability to phase lock to stimuli, as the vector strengths for both WT and mutant animals were similar across all stimulation frequencies (Figure 6D). Similarly, the measured preferred phase angles were indistinguishable among genotypes. Figure 6E shows that the latency to the first response was also unchanged in mutant animals.

DISCUSSION

Evidence for Ribeye Forming the Core of the Ribbon

In this study, we used genome editing techniques to introduce mutations into the coding regions of the synaptic ribbon-specific A-domain of both zebrafish *ribeye* genes. Mutant animals exhibit greatly reduced levels of Ribeye, leading to striking morphological changes to the synaptic ribbons of hair cells. In particular, double-homozygous mutants have ribbons that lack the central electron density while maintaining a roughly spherical scaffold that harbors attached synaptic vesicles. Of note, the ghost ribbons were found to have lost 66% of their estimated volume, similar to the estimated contribution of Ribeye to ribbon volume in bipolar cells (Zenisek et al., 2004) but considerably more than the volume occupied by the density in micrographs. Previous studies have demonstrated that overexpressed Ribeye forms electron-dense aggregates in HEK and R28 cells (Schmitz et al., 2000; Magupalli et al., 2008) and leads to ectopic electron densities in neuromast hair cells (Sheets et al., 2011). In some systems, the A-domain alone is sufficient to form densities, whereas the B-domain alone forms a soluble protein (Schmitz et al., 2000). Summed together, it is reasonable to conclude that the core density observed in electron micrographs of synaptic ribbons is largely composed of the A-domain of Ribeye protein, whereas the surrounding halo of lighter material is made

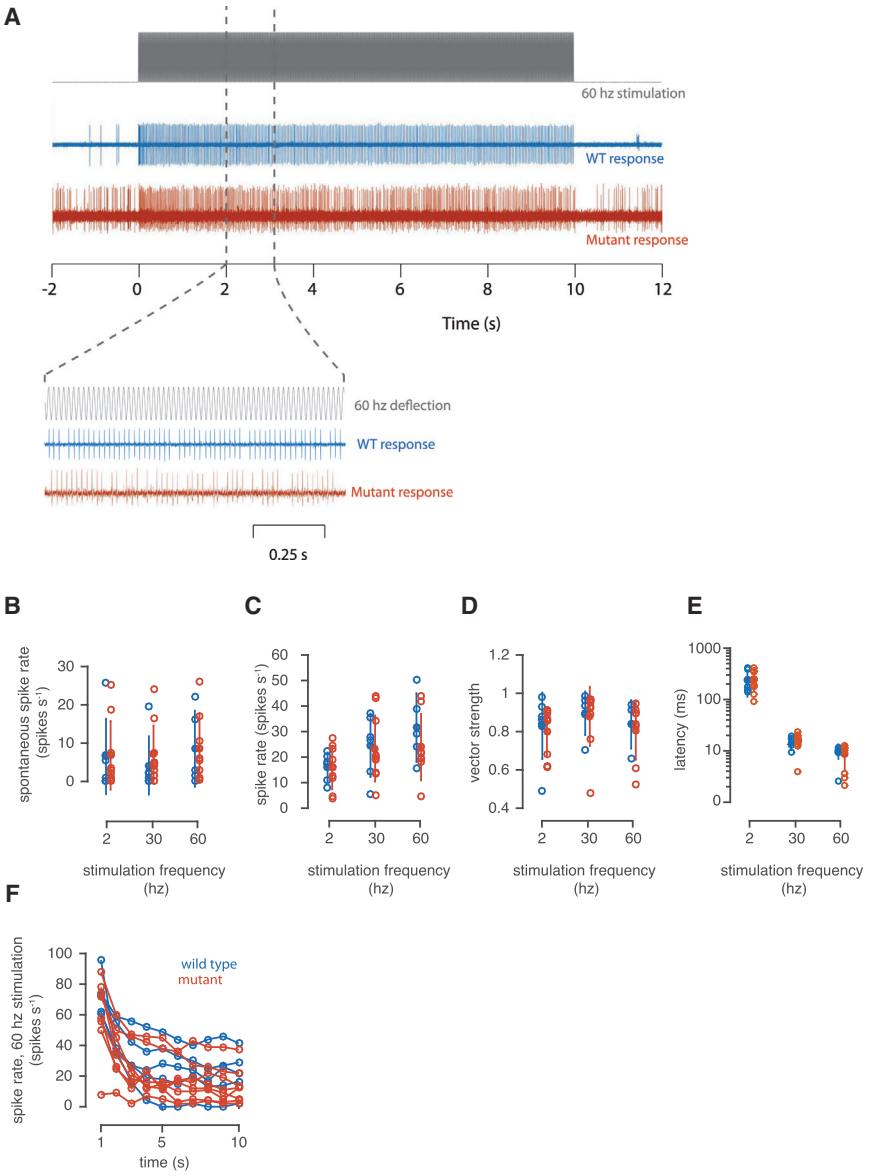

Figure 6. Electrophysiology Recordings from the Primary Afferent Neurons of Lateral Line Neuromasts

(A) Representative traces showing the spiking rates for the afferent neurons of WT (blue) and mutant (red) zebrafish in response to 10 s of 60-Hz sine wave stimulation.

(B) The spontaneous spike rate measured for WT and mutant animals before stimulation.

(C) The average spike rate calculated over the entire 10 s of stimulation for stimulation frequencies of 2, 30, and 60 Hz.

(D) The average vector strength calculated for the entire 10 s of stimulation.

(E) The latency between the onset of stimulation and the first spike.

(F) The spike rate as a function of time during 10 s of 60 Hz stimulation. Closed circles show the mean; error bars indicate SD.

up of the B-domain of Ribeye along with other ribbon proteins that remain in place in our mutant animals. This idea is consistent with the original model put forth by Schmitz, Sudhof, and colleagues (Schmitz et al., 2000).

We find that most "ghost ribbons," while smaller, appear to take on a shape that is similar to that of normal ribbons (although see Figures 3C–3F) and still retain a scaffold capable of recruiting vesicles. Interestingly, we found two examples of ghost-ribbon-like structures in photoreceptors of mutant mice, which appeared more elongated than the hair cell ghost ribbons, mimicking the structure of photoreceptor ribbons. It remains possible that the sparse Ribeye remaining in these cells may maintain the structure but fail to form a density. Alternatively, numerous structural proteins have been shown to localize to the ribbon complex (Brandstätter et al., 1999), including Piccolo, Bassoon, Cast/ERC, Rim1, and Rim2, but each of these proteins is also found at conventional synapses, which lack the ribbon structure. Of note, a ribbon-specific isoform of Piccolo has been described in retina (Regus-Leidig et al., 2013, 2014b), suggesting that ribbon-specific splicing may underlie some of the diversity in ribbon shape and size.

It is noteworthy that some of the features we report here differ from those found in a recent report characterizing retinal ribbons in Ribeye knockout mice (Maxeiner et al., 2016). In that study, the authors found ribbons completely lacking from the retina and a general decrease in vesicles residing near active zones. Additionally, they found that synaptic transmission between rod bipolar cells and AII Amacrine cells was reduced by approximately 80%, whereas in our study, exocytosis, measured by capacitance, is slightly enhanced. As in our study, the kinetics of the responses remained unchanged, suggesting that ribbons are not required to maintain continuous release from bipolar cells. Although the reasons for the differences in the two studies are unknown at this point, we hypothesize several possible explanations. (1) In our study, a small amount of Ribeye remains in hair cells, which may be sufficient to nucleate the ghost-ribbon structures and be sufficient to stabilize synaptic structures containing other ribbon proteins. (2) Occult ghost ribbons might account for 20% of release from mouse bipolar cells. Ghost ribbons lack the electron density and are smaller than WT ribbons and, thus, were initially difficult to find in electron micrographs in neuromast hair cells. Identifying such structures in mouse bipolar cells ribbons would be even more difficult, since bipolar cell ribbons are smaller and vesicles are found at high densities throughout the cytoplasm. Moreover, since release is reduced by 80%, ghost-ribbon

numbers may be similarly reduced. (3) The differences may reflect species- and/or tissue-specific roles for Ribeye.

Relationship between Ribeye and Vesicles

In this study, we find that ghost ribbons possess an estimated 50% of the surface area of WT ribbons, while maintaining near-normal vesicle numbers. Physical tethers linking the ribbon to synaptic vesicles are observable in some electron micrographs (e.g., Lenzi et al., 2002), but the molecular components of the tether remain obscure. Since vesicle numbers remain constant, despite dramatic reductions in Ribeye levels, we posit that a yet-to-be-identified protein may link vesicles to ribbons and that loss of ribbon volume results in an increase in concentration of this molecule on the ribbon. Our results here argue against Ribeye directly participating in the tethering of synaptic vesicles.

Synaptic vesicles associated with ghost ribbons were also found to be smaller than those associated with ribbons in WT animals. The reasons for this difference is currently unknown, but it is worth noting that Ribeye has been suggested to act as a lyosphosphatidyl acyl tranferase that adds an acyl group to lysolipids, thus converting lysophosphophatidic acid (LPA) with one acyl chain to phosphatidic acid (PA) with two acyl chains (Schwarz et al., 2011). Since the LPA and PA have opposite effects on membrane curvature, the acyltransferase activity has the potential to influence membrane curvature and, by extension, vesicle size.

Ribeye, Synaptic Localization, and Calcium Channels

Prior to the present study, several lines of evidence have pointed toward a close relationship between Ribeye and calcium channels in ribbon synapses. Calcium channels have been shown to localize to clusters beneath the ribbon in ribbon synapses (Roberts et al., 1990; Zenisek et al., 2003; Frank et al., 2010). Moreover, the tight coupling of fast exocytosis to calcium channels appears to be a feature of many ribbon synapses (Singer and Diamond, 2003; Mennerick and Matthews, 1996; Moser and Beutner, 2000; Wong et al., 2014). A link between Ribeye and calcium channels has previously been inferred from overexpression and knockdown studies in zebrafish. MO-driven knockdown of ribeye leads to loss of calcium channel clusters in both retina (Lv et al., 2012) and neuromast hair cells (Sheets et al., 2012), whereas animals overexpressing Ribeye exhibit ectopic calcium channel clusters that colocalize with Ribeye protein aggregates (Sheets et al., 2012). More recently, knockout of Ribeye in mouse was found to cause a subtle change in the size of calcium channel clusters in photoreceptors (Maxeiner et al., 2016). Notably, in contrast to the previous MO results in retina (Lv et al., 2012), calcium channels remained clustered in discrete locations in the retina. Additionally, knockout mice were found to exhibit an increase in sensitivity of mEPSC frequency to high levels of the membrane-permeant analog of EGTA, EGTA-AM. Since mEPSC frequency is also reduced by calcium channel blockers (Mehta et al., 2013; Maxeiner et al., 2016), the results were suggestive of a loss of coupling between calcium channels and release sites.

Here, we show that genetic disruption of Ribeye expression leads to mislocalization and redistribution of calcium channels in neuromast hair cells, in line with the previous work using MOs (Sheets et al., 2012). This redistribution of calcium channels is associated with a slight enhancement of calcium current. Although the reason for the increase in calcium current is unknown at present, we posit that homeostatic plasticity, in response to less neurotransmitter released on to afferent fibers, may trigger an upregulation of calcium current and exocytosis in these cells, similar to what has been described for other systems (Frank, 2014). Alternatively, Ribeye may act as a negative regulator of voltage-gated calcium channel expression or activity, with the latter being a distinct possibility, given that CtBP2 functions as a co-repressor. Further work will be necessary to determine the mechanisms behind the enhanced calcium current observed here. We also show here that the continuous phase of exocytosis in mutant animals exhibits an enhanced sensitivity to EGTA. Mutant hair cells retain an EGTA-insensitive component of release that retains similar exponential release kinetics, suggesting that some vesicles may still reside in nanodomains near calcium channels.

Of note, inner hair cells from mice harboring mutations to the synaptic ribbon protein Bassoon, which exhibit few ribbons that associate with the plasma-membrane exhibit a reduction in voltage-gated calcium current. Interestingly, a small subset of ribbons in Bsn mice associates with the plasma membrane at synapses, and these synapses exhibit more calcium channels than ribbon-less synapses (Frank et al., 2010). The opposite effect on calcium current in Bassoon mice, compared with *re[a(Δ10)/b(Δ7)]* double-homozygous fish, may indicate that the two proteins interact with and regulate calcium channels differently, with Bassoon influencing overall expression level or channel stability and Ribeye having an effect on channel localization.

Interestingly, several studies have demonstrated that mutations to calcium channel subunits have a reciprocal effect on synaptic ribbon morphology, although the magnitude and specific effects have varied between preparations. For example, a mutation in the zebrafish gene encoding for the alpha subunit of Cav 1.4 channels results in the disappearance of cone synaptic ribbons (Jia et al., 2014), whereas genetic or pharmacological removal of calcium conductance through Cav 1.3 channels increases the size of ribbons in lateral line hair cells (Sheets et al., 2012). In mouse, the genetic removal of Cav1.4 channels prevents the formation of mature synaptic ribbons (Liu et al., 2013; Regus-Leidig et al., 2014a), whereas Cav1.3 is not required for the generation or maturation of auditory hair cell ribbons but is required for proper maintenance of the synapses (Nemzou N et al., 2006).

Effects on Synaptic Transmission

Here, our results show an enhanced continuous phase of exocytosis in animals deficient in Ribeye. Given that there are fewer ghost ribbons than WT ribbons and that most ghost ribbons fail to localize to proper synaptic locations, we suggest that much of this continuous phase of release may arise from extra-ribbon locations. Our results are in line with several imaging and electrophysiological studies that have demonstrated that extra-ribbon release can occur in ribbon-bearing cells during prolonged stimulation (Mehta et al., 2014; Zenisek et al., 2000; Midorikawa et al., 2007; Pangršič et al., 2015; Chen et al.,

Please cite this article in press as: Lv et al., Synaptic Ribbons Require Ribeye for Electron Density, Proper Synaptic Localization, and Recruitment of Calcium Channels, Cell Reports (2016), http://dx.doi.org/10.1016/j.celrep.2016.05.045

2013). We do not suggest, however, that synaptic transmission does not normally occur at ribbon locations in wild-type animals, since direct lines of evidence have firmly established exocytosis at ribbon sites (Vaithianathan et al., 2016; Zenisek, 2008; Chen et al., 2013; Midorikawa et al., 2007).

In contrast to our results here, acute inactivation of the synaptic ribbon using fluorophore-assisted light inactivation (FALI) of ribbon-targeted fluorescent peptides cause the loss of spontaneous and both fast and slow components of evoked release (Mehta et al., 2013; Snellman et al., 2011). Although the peptides used in those studies specifically target Ribeye, FALI generates a sphere of damage likely to also include local bystander proteins associated with the synaptic ribbon. The comparatively mild changes to release properties in cells missing Ribeye implicate these other nearby proteins in functions essential for maintaining focal neurotransmitter release in these cells. Indeed, ghost ribbons maintain a shape and vesicle clusters that resemble WT ribbons, suggesting that many ribbon-resident proteins inhabit these structures in mutant animals. Relatedly, inner hair cells from mice harboring mutations to Bassoon show decreases in both transient (Khimich et al., 2005) and sustained (Frank et al., 2010) components of exocytosis. This comparatively greater effect of Bassoon removal suggests that either Bassoon itself or proteins recruited by Bassoon to ribbons play a more fundamental role in determining release properties from ribbon synapses. Indeed, the genetic disruption of Bassoon causes a change in open probability, reduces channel number, and causes a redistribution of calcium channels in hair cells (Frank et al., 2010). The effect of Bassoon removal must overwhelm any homeostatic compensatory mechanisms that might normally return calcium current to normal levels. In addition to Bassoon, several other proteins already known to have critical functions in conventional synapses have been demonstrated to localize either to the ribbon or the plasma membrane beneath the ribbon (Regus-Leidig and Brandstatter, 2011; tom Dieck et al., 2005).

Surprisingly, despite the loss of efficient coupling between calcium channels and release sites in mutants and reduction in ribbon numbers, we could detect no differences in afferent responses. Spontaneous and evoked release rates at three different frequencies, the latency to first spike and the ability to phase lock were indistinguishable between genotypes. A key difference in capacitance measurements and afferent spike recordings is that afferent recordings are dependent upon exocytosis at specific locations, namely, on to receptors populating afferent fibers, whereas capacitance recordings have no such spatial requirements. As such capacitance measurements reflect both synaptic and extrasynaptic release. Similar to our results, hair cells in mice lacking endogenous calcium-binding proteins show enhanced continuous release, without an effect on afferent responses, consistent with extrasynaptic release contributing significantly to capacitance response (Pangršič et al., 2015). Given that, in the presence of 10 mM EGTA, some exocytosis persists with normal kinetics in mutant animals, we suggest that this EGTA-resistant component represents the subset of vesicles, which is properly localized near calcium channels, and could be sufficient to drive afferent neuron spiking to near normal levels for afferents that receive synaptic input. It should be noted that, to perform afferent recordings, one first identifies and selects for synaptically connected neurons before performing experiments. Thus, recordings represent only those neurons, which generate spikes in response to mechanical stimuli to hair cells, and cannot account for cells that lack synaptic connections. These results suggest that when synapses with ghost ribbons are formed, they respond to stimuli normally under the conditions we tested. It should also be noted that while the stimulus frequencies we tested here are typical or slightly higher for neuromast hair cells, auditory hair cells of the inner ear respond to much higher frequencies and exhibit faster kinetics and greater demands on neurotransmitter release. Because of this, the faster hair cells of other systems may show greater defects in the absence of Ribeye.

EXPERIMENTAL PROCEDURES

Zebrafish Husbandry

Zebrafish were kept in accordance with the Yale University Animal Care and Use Committee guidelines.

Generation of *ribeye a* Mutant Fish

Ribeye a mutant fish were generated using zinc finger nucleases (ZFNs) targeting the A-domain of Ribeye a (ENSDARG00000044062) purchased from Sigma-Aldrich. mRNAs encoding the ZFNs were injected into one-cell-stage embryos, and progeny were screened for mutations. Mutants (Figure S1) were selected for breeding to generate homozygous mutants. Detailed experimental procedures are provided in the Supplemental Experimental Procedures.

Generation of *ribeye b* Mutant Fish

CRISPR/Cas9-induced mutagenesis procedures were adapted from previously published reports (Hruscha et al., 2013) and are detailed in the Supplemental Experimental Procedures. Single guide RNAs (sgRNAs) were designed to target to the Ribeye-specific A-domain of *ribeye b*. Several mutant lines were identified and selected for further study (Figure S2).

EM and Immunofluorescence

Procedures were adapted from standard previously published experimental protocols (Obholzer et al., 2008; Lv et al., 2012) and are detailed in the Supplemental Experimental Procedures.

Hair-Cell Voltage-Clamp Recordings

Whole-cell voltage-clamp recordings were carried out from neuromast hair cells in anesthetized live zebrafish (5–7 dpf), as previously described (Ricci et al., 2013). Details can be found in the Supplemental Experimental Procedures.

Afferent Neuron Recordings

Loose-patch recordings from soma of afferent neurons were made on anesthetized and paralyzed larval zebrafish as previously described and detailed in the Supplemental Experimental Procedures (Levi et al., 2015).

Statistical Analysis

Data are presented as mean ± SEM. Statistical significance across datasets was determined using the unpaired two-tailed t test. Significance was considered $p < 0.05$; however, for most comparisons in the present study, $p < 0.01$.

SUPPLEMENTAL INFORMATION

Supplemental Information includes Supplemental Experimental Procedures and two figures and can be found with this article online at http://dx.doi.org/10.1016/j.celrep.2016.05.045.

AUTHOR CONTRIBUTIONS

C.L. designed and conducted experiments, analyzed data, and wrote the paper; W.J.S. performed experiments, analyzed data, and participated in the writing; O.A. analyzed data and participated in the writing; C.F. analyzed morphological data; J.Z. analyzed electrophyiological data; J.S.-S. analyzed data and provided technical expertise; L.S. performed experiments, analyzed data, and participated in writing; J.C.L. oversaw afferent recording experiments and interpreted and analyzed data; D.Z. designed experiments, analyzed data, and wrote the paper.

ACKNOWLEDGMENTS

This work was funded by NIH grants EY021195 (to D.Z.), DC008130 (to J.S.-S.), and DC010809 (to J.C.L.); the Amelia Peabody Charitable Fund (to L.S.); and National Science Foundation grant IOS1257150 (to J.C.L.).

Received: July 30, 2015
Revised: April 6, 2016
Accepted: May 10, 2016
Published: June 9, 2016

REFERENCES

Adler, E.M., Augustine, G.J., Duffy, S.N., and Charlton, M.P. (1991). Alien intracellular calcium chelators attenuate neurotransmitter release at the squid giant synapse. J. Neurosci. *11*, 1496–1507.

Bartoletti, T.M., Babai, N., and Thoreson, W.B. (2010). Vesicle pool size at the salamander cone ribbon synapse. J. Neurophysiol. *103*, 419–423.

Brandstätter, J.H., Fletcher, E.L., Garner, C.C., Gundelfinger, E.D., and Wässle, H. (1999). Differential expression of the presynaptic cytomatrix protein bassoon among ribbon synapses in the mammalian retina. Eur. J. Neurosci. *11*, 3683–3693.

Chen, M., Van Hook, M.J., Zenisek, D., and Thoreson, W.B. (2013). Properties of ribbon and non-ribbon release from rod photoreceptors revealed by visualizing individual synaptic vesicles. J. Neurosci. *33*, 2071–2086.

Coggins, M., and Zenisek, D. (2009). Evidence that exocytosis is driven by calcium entry through multiple calcium channels in goldfish retinal bipolar cells. J. Neurophysiol. *101*, 2601–2619.

Edmonds, B.W., Gregory, F.D., and Schweizer, F.E. (2004). Evidence that fast exocytosis can be predominantly mediated by vesicles not docked at active zones in frog saccular hair cells. J. Physiol. *560*, 439–450.

Eisen, M.D., Spassova, M., and Parsons, T.D. (2004). Large releasable pool of synaptic vesicles in chick cochlear hair cells. J. Neurophysiol. *91*, 2422–2428.

Frank, C.A. (2014). How voltage-gated calcium channels gate forms of homeostatic synaptic plasticity. Front. Cell. Neurosci. *8*, 40.

Frank, T., Rutherford, M.A., Strenzke, N., Neef, A., Pangršič, T., Khimich, D., Fejtova, A., Gundelfinger, E.D., Liberman, M.C., Harke, B., et al. (2010). Bassoon and the synaptic ribbon organize Ca^2+ channels and vesicles to add release sites and promote refilling. Neuron *68*, 724–738.

Hruscha, A., Krawitz, P., Rechenberg, A., Heinrich, V., Hecht, J., Haass, C., and Schmid, B. (2013). Efficient CRISPR/Cas9 genome editing with low off-target effects in zebrafish. Development *140*, 4982–4987.

Jia, S., Muto, A., Orisme, W., Henson, H.E., Parupalli, C., Ju, B., Baier, H., and Taylor, M.R. (2014). Zebrafish Cacna1fa is required for cone photoreceptor function and synaptic ribbon formation. Hum. Mol. Genet. *23*, 2981–2994.

Khimich, D., Nouvian, R., Pujol, R., Tom Dieck, S., Egner, A., Gundelfinger, E.D., and Moser, T. (2005). Hair cell synaptic ribbons are essential for synchronous auditory signalling. Nature *434*, 889–894.

Lagnado, L., Gomis, A., and Job, C. (1996). Continuous vesicle cycling in the synaptic terminal of retinal bipolar cells. Neuron *17*, 957–967.

Lenzi, D., Crum, J., Ellisman, M.H., and Roberts, W.M. (2002). Depolarization redistributes synaptic membrane and creates a gradient of vesicles on the synaptic body at a ribbon synapse. Neuron *36*, 649–659.

Levi, R., Akanyeti, O., Ballo, A., and Liao, J.C. (2015). Frequency response properties of primary afferent neurons in the posterior lateral line system of larval zebrafish. J. Neurophysiol. *113*, 657–668.

Liu, X., Kerov, V., Haeseleer, F., Majumder, A., Artemyev, N., Baker, S.A., and Lee, A. (2013). Dysregulation of Ca(v)1.4 channels disrupts the maturation of photoreceptor synaptic ribbons in congenital stationary night blindness type 2. Channels (Austin) *7*, 514–523.

Lv, C., Gould, T.J., Bewersdorf, J., and Zenisek, D. (2012). High-resolution optical imaging of zebrafish larval ribbon synapse protein RIBEYE, RIM2, and CaV 1.4 by stimulation emission depletion microscopy. Microsc. Microanal. *18*, 745–752.

Magupalli, V.G., Schwarz, K., Alpadi, K., Natarajan, S., Seigel, G.M., and Schmitz, F. (2008). Multiple RIBEYE-RIBEYE interactions create a dynamic scaffold for the formation of synaptic ribbons. J. Neurosci. *28*, 7954–7967.

Matthews, G., and Fuchs, P. (2010). The diverse roles of ribbon synapses in sensory neurotransmission. Nat. Rev. Neurosci. *11*, 812–822.

Maxeiner, S., Luo, F., Tan, A., Schmitz, F., and Südhof, T.C. (2016). How to make a synaptic ribbon: RIBEYE deletion abolishes ribbons in retinal synapses and disrupts neurotransmitter release. EMBO J., e201592701.

Mehta, B., Snellman, J., Chen, S., Li, W., and Zenisek, D. (2013). Synaptic ribbons influence the size and frequency of miniature-like evoked postsynaptic currents. Neuron *77*, 516–527.

Mehta, B., Ke, J.B., Zhang, L., Baden, A.D., Markowitz, A.L., Nayak, S., Briggman, K.L., Zenisek, D., and Singer, J.H. (2014). Global Ca2+ signaling drives ribbon-independent synaptic transmission at rod bipolar cell synapses. J. Neurosci. *34*, 6233–6244.

Mennerick, S., and Matthews, G. (1996). Ultrafast exocytosis elicited by calcium current in synaptic terminals of retinal bipolar neurons. Neuron *17*, 1241–1249.

Meyer, M.P., Trimmer, J.S., Gilthorpe, J.D., and Smith, S.J. (2005). Characterization of zebrafish PSD-95 gene family members. J. Neurobiol. *63*, 91–105.

Midorikawa, M., Tsukamoto, Y., Berglund, K., Ishii, M., and Tachibana, M. (2007). Different roles of ribbon-associated and ribbon-free active zones in retinal bipolar cells. Nat. Neurosci. *10*, 1268–1276.

Moser, T., and Beutner, D. (2000). Kinetics of exocytosis and endocytosis at the cochlear inner hair cell afferent synapse of the mouse. Proc. Natl. Acad. Sci. USA *97*, 883–888.

Nemzou N, R.M., Bulankina, A.V., Khimich, D., Giese, A., and Moser, T. (2006). Synaptic organization in cochlear inner hair cells deficient for the CaV1.3 (alpha1D) subunit of L-type Ca2+ channels. Neuroscience *141*, 1849–1860.

Obholzer, N., Wolfson, S., Trapani, J.G., Mo, W., Nechiporuk, A., Busch-Nentwich, E., Seiler, C., Sidi, S., Söllner, C., Duncan, R.N., et al. (2008). Vesicular glutamate transporter 3 is required for synaptic transmission in zebrafish hair cells. J. Neurosci. *28*, 2110–2118.

Pangršič, T., Gabrielaitis, M., Michanski, S., Schwaller, B., Wolf, F., Strenzke, N., and Moser, T. (2015). EF-hand protein Ca2+ buffers regulate Ca2+ influx and exocytosis in sensory hair cells. Proc. Natl. Acad. Sci. USA *112*, E1028–E1037.

Parsons, T.D., Lenzi, D., Almers, W., and Roberts, W.M. (1994). Calcium-triggered exocytosis and endocytosis in an isolated presynaptic cell: capacitance measurements in saccular hair cells. Neuron *13*, 875–883.

Regus-Leidig, H., and Brandstatter, J.H. (2011). Structure and function of a complex sensory synapse. Acta Physiol. (Oxf.) *204*, 479–486.

Regus-Leidig, H., Ott, C., Löhner, M., Atorf, J., Fuchs, M., Sedmak, T., Kremers, J., Fejtová, A., Gundelfinger, E.D., and Brandstätter, J.H. (2013). Identification and immunocytochemical characterization of Piccolino, a novel Piccolo splice variant selectively expressed at sensory ribbon synapses of the eye and ear. PLoS ONE *8*, e70373.

Regus-Leidig, H., Atorf, J., Feigenspan, A., Kremers, J., Maw, M.A., and Brandstätter, J.H. (2014a). Photoreceptor degeneration in two mouse models for congenital stationary night blindness type 2. PLoS ONE *9*, e86769.

Please cite this article in press as: Lv et al., Synaptic Ribbons Require Ribeye for Electron Density, Proper Synaptic Localization, and Recruitment of Calcium Channels, Cell Reports (2016), http://dx.doi.org/10.1016/j.celrep.2016.05.045

Regus-Leidig, H., Fuchs, M., Löhner, M., Leist, S.R., Leal-Ortiz, S., Chiodo, V.A., Hauswirth, W.W., Garner, C.C., and Brandstätter, J.H. (2014b). In vivo knockdown of Piccolino disrupts presynaptic ribbon morphology in mouse photoreceptor synapses. Front. Cell. Neurosci. *8*, 259.

Ricci, A.J., Bai, J.P., Song, L., Lv, C., Zenisek, D., and Santos-Sacchi, J. (2013). Patch-clamp recordings from lateral line neuromast hair cells of the living zebrafish. J. Neurosci. *33*, 3131–3134.

Roberts, W.M. (1994). Localization of calcium signals by a mobile calcium buffer in frog saccular hair cells. J. Neurosci. *14*, 3246–3262.

Roberts, W.M., Jacobs, R.A., and Hudspeth, A.J. (1990). Colocalization of ion channels involved in frequency selectivity and synaptic transmission at presynaptic active zones of hair cells. J. Neurosci. *10*, 3664–3684.

Schmitz, F., Königstorfer, A., and Südhof, T.C. (2000). RIBEYE, a component of synaptic ribbons: a protein's journey through evolution provides insight into synaptic ribbon function. Neuron *28*, 857–872.

Schnee, M.E., Santos-Sacchi, J., Castellano-Muñoz, M., Kong, J.H., and Ricci, A.J. (2011). Calcium-dependent synaptic vesicle trafficking underlies indefatigable release at the hair cell afferent fiber synapse. Neuron *70*, 326–338.

Schwarz, K., Natarajan, S., Kassas, N., Vitale, N., and Schmitz, F. (2011). The synaptic ribbon is a site of phosphatidic acid generation in ribbon synapses. J. Neurosci. *31*, 15996–16011.

Sheets, L., Trapani, J.G., Mo, W., Obholzer, N., and Nicolson, T. (2011). Ribeye is required for presynaptic Ca(V)1.3a channel localization and afferent innervation of sensory hair cells. Development *138*, 1309–1319.

Sheets, L., Kindt, K.S., and Nicolson, T. (2012). Presynaptic CaV1.3 channels regulate synaptic ribbon size and are required for synaptic maintenance in sensory hair cells. J. Neurosci. *32*, 17273–17286.

Singer, J.H., and Diamond, J.S. (2003). Sustained Ca2+ entry elicits transient postsynaptic currents at a retinal ribbon synapse. J. Neurosci. *23*, 10923–10933.

Snellman, J., Mehta, B., Babai, N., Bartoletti, T.M., Akmentin, W., Francis, A., Matthews, G., Thoreson, W., and Zenisek, D. (2011). Acute destruction of the synaptic ribbon reveals a role for the ribbon in vesicle priming. Nat. Neurosci. *14*, 1135–1141.

tom Dieck, S., Altrock, W.D., Kessels, M.M., Qualmann, B., Regus, H., Brauner, D., Fejtová, A., Bracko, O., Gundelfinger, E.D., and Brandstätter, J.H. (2005). Molecular dissection of the photoreceptor ribbon synapse: physical interaction of Bassoon and RIBEYE is essential for the assembly of the ribbon complex. J. Cell Biol. *168*, 825–836.

Vaithianathan, T., Henry, D., Akmentin, W., and Matthews, G. (2016). Nanoscale dynamics of synaptic vesicle trafficking and fusion at the presynaptic active zone. eLife *5*, 13245.

Wong, A.B., Rutherford, M.A., Gabrielaitis, M., Pangrsic, T., Göttfert, F., Frank, T., Michanski, S., Hell, S., Wolf, F., Wichmann, C., and Moser, T. (2014). Developmental refinement of hair cell synapses tightens the coupling of Ca2+ influx to exocytosis. EMBO J. *33*, 247–264.

Zenisek, D. (2008). Vesicle association and exocytosis at ribbon and extraribbon sites in retinal bipolar cell presynaptic terminals. Proc. Natl. Acad. Sci. USA *105*, 4922–4927.

Zenisek, D., Steyer, J.A., and Almers, W. (2000). Transport, capture and exocytosis of single synaptic vesicles at active zones. Nature *406*, 849–854.

Zenisek, D., Davila, V., Wan, L., and Almers, W. (2003). Imaging calcium entry sites and ribbon structures in two presynaptic cells. J. Neurosci. *23*, 2538–2548.

Zenisek, D., Horst, N.K., Merrifield, C., Sterling, P., and Matthews, G. (2004). Visualizing synaptic ribbons in the living cell. J. Neurosci. *24*, 9752–9759.